Ocean Engineering 297 (2024) 117012

Contents lists available at ScienceDirect

Ocean Engineering

journal homepage: www.elsevier.com/locate/oceaneng

Optimized design and analysis of cable-based parallel manipulators for enhanced subsea operations

Asim Ghaffar [a], Muhammad Zia Ur Rahman [a], Víctor Leiva [b,*], Cecilia Castro [c]

[a] Department of Mechanical, Mechatronics and Manufacturing Engineering, University of Engineering and Technology Lahore, Faisalabad Campus, Faisalabad, Pakistan
[b] School of Industrial Engineering, Pontificia Universidad Católica de Valparaíso, Valparaíso, Chile
[c] Centre of Mathematics, Universidade do Minho, Braga, Portugal

ARTICLE INFO

Keywords:
Dykstra algorithm
Layout optimization
Stiffness modeling
Subsea environments

ABSTRACT

The subsea exploration of complex and challenging areas has increased the need for advanced robotic frameworks, such as cable-based parallel manipulators (CPMs). Known for their flexibility and precision, CPMs are essential for performing detailed tasks underwater. In submarine environments, handling external underwater forces presents a significant challenge, necessitating the optimization of cable tension for effective operation of CPMs. Additionally, achieving a balance between an increased workspace volume and improved manipulator stiffness is crucial. Addressing these challenges, this article presents a design and optimization approach for CPMs. The focus is on the eight- and ten-cable configurations, specifically chosen for their optimal balance of complexity and control. To enhance the efficiency and effectiveness of CPMs in these demanding environments, the article proposes several optimizations, including adjustments in workspace dynamics, cable tension, system layout, and manipulator stiffness. The proposed methodology involves innovative approaches, including an adaptation of the Dykstra algorithm, to refine cable tension optimization, and explores layout optimization strategies to achieve an ideal balance between enlarged workspace and enhanced manipulator stiffness. A key aspect of the present research is the stiffness analysis via natural frequencies, establishing an essential link between detailed design choices and overall manipulator performance. The findings reveal that meticulous design and optimization of CPMs significantly enhance operational efficiency, range, and stability in underwater environments. These advancements provide valuable insights for the broader application of cable-based manipulators in complex underwater tasks, establishing new benchmarks in the field and laying the foundation for future innovations in underwater robotic systems.

1. Introduction

The field of robotics is continually evolving, introducing manipulator designs in diverse applications (Ghaffar et al., 2024). In this diversity, cable-based parallel manipulators (CPMs), which are robotic systems that operate using cables for movement and control, have emerged as a solution, offering flexibility, precision, and benefits in challenging environments (Ghaffar and Hassan, 2015b; Alakhras et al., 2022; Nazir et al., 2022; Hamdoun et al., 2017; Wang et al., 2021; Juárez-Pérez et al., 2022; Muntashir and Nurahmi, 2022).

In subaquatic operations with environments unpredictable, the capabilities of CPMs become significant. These manipulators, optimized for marine settings, excel tasks such as marine archaeology, offshore maintenance, salvage operations, and seabed mapping (Zhang et al., 2020a; Poitrimol and Igarashi, 2020; Ou et al., 2022; Sawai et al., 2019; Horoub et al., 2023; Mazzeo et al., 2022).

Recent advancements in the dynamic modeling and control of underwater manipulators have enhanced their applicability in marine operations. The work presented in Shang et al. (2024) explored underwater environments in relation to the impact of flowing water on operational accuracy, and proposed corresponding control strategies. The insights obtained from the mentioned works into the dynamic behavior of underwater manipulators in various conditions are relevant to the ongoing development of CPMs, emphasizing the need for control mechanisms in unpredictable marine environments.

Optimizing system layouts in subsea environments, as investigated in Yue et al. (2023), provides a valuable perspective for deploying CPMs. In this line of work, one can consider factors like hydraulic pressure loss and seabed terrain, which influence the efficiency and effectiveness of CPMs in underwater tasks.

* Corresponding author.
E-mail addresses: victorleivasanchez@gmail.com (V. Leiva), cecilia@math.uminho.pt (C. Castro).

https://doi.org/10.1016/j.oceaneng.2024.117012
Received 29 November 2023; Received in revised form 1 February 2024; Accepted 2 February 2024
Available online 14 February 2024

The related literature addresses diverse innovative settings in the design of CPMs (Williams and Graf, 2020; Maeda et al., 1999; Shen et al., 2021; Ferraresi et al., 2004; Xiong et al., 2020). Key aspects of these designs include workspace evaluation (Cui and Tang, 2021; Zarebidoki et al., 2022; Tho and Thinh, 2022; Jin et al., 2023; Zhang et al., 2020b), stiffness modeling (Cui et al., 2019; Gueners et al., 2021; Ahmad et al., 2011), and the behavior of cables under different conditions (Pierri et al., 2020; Hassan and Khajepour, 2011; Su et al., 2023). Optimizing cable tensions in response to external forces is a crucial area of research (Wahba and Honig, 2023), with recent studies exploring fractional transformation-based control methods to enhance the manipulator responsiveness and robustness (Rahman et al., 2022a,b). The integration of fractional transformation in this area is a promising direction for future research, as it could improve the control and robustness of such systems (Rahman et al., 2023b).

Despite extensive research in the field of CPMs, there remains a gap in understanding how these manipulators can be optimized for the unique dynamics and challenges of deep-sea environments. Existing studies have focused on the basic design and functionality of CPMs without exploring how they perform under the unpredictable conditions of marine environments stating a gap in the literature on the topic.

The present study is among the first to address the mentioned gap, aiming to enhance the stability, efficiency, and adaptability of CPMs in challenging underwater conditions. Accordingly, the primary objective of this research is to propose a methodology that enhances the operational efficiency and adaptability of CPMs within dynamic marine environments. The focus of this investigation is on refining the design and functionality of CPMs to address the varying forces prevalent in such environments. This allows CPMs to adapt and maintain effectiveness amidst the unpredictable and challenging conditions of the deep sea. Particular attention is given to the eight- and ten-cable configurations, which have been selected for their optimal balance of complexity and control.

This work considers factors like hydraulic pressure loss and seabed terrain, which influence the efficiency and effectiveness of CPMs in underwater tasks. The present research centers on analyzing the kinematic and dynamic behavior of CPMs considering various underwater conditions. It investigates the effects of varying cable tensions and ship placements on the manipulator range of motion, stability, and responsiveness to external forces such as ocean currents. Furthermore, the study introduces new optimization algorithms, including adaptations of the Dykstra projection algorithm (Dykstra, 1983), to balance cable tensions with manipulator positioning. This algorithm was chosen due to its robustness and effectiveness in dealing with the non-linear, multidimensional optimization problems (Hamidi et al., 2023), a characteristic that is usual in underwater manipulator dynamics. The Dykstra algorithm is effective in situations where precise control and adaptability to changing conditions are requested. This makes the Dykstra algorithm a good choice for dealing with the various forces that affect CPMs in underwater operations.

The proposed research also examines how increasing the number of cables and how using different ship configurations can affect the working space and firmness of the manipulators. By changing these number and configurations, the study seeks to uncover better design strategies that can improve the tasks under water.

The new methodology is built on existing research, including model-based control methods for complex systems, as discussed in Rahman et al. (2023c). The proposed methodology extends foundational research in the field, drawing on methods used in cable-based systems for underwater applications (Ghaffar and Hassan, 2014) and ship position optimization for cable-based manipulators (Ghaffar and Hassan, 2015a). This investigation is innovative in its thorough exploration of how CPMs work and how they respond to the challenges of the marine environment, contributing significantly to the advancement of knowledge in marine robotics.

The study is anticipated to provide important insights into the design and operation of CPMs, thereby improving their performance in marine tasks. In comparison to previous research that focused mainly on CPM design, this study incorporates environmental considerations into the design process, offering a unique contribution to the field.

In summary, the present investigation fills the identified gap in the literature and brings new perspectives to design and optimize cable-based manipulators for underwater use. The investigation lays the groundwork for future developments in underwater robotics, charting a path for innovative oceanic research.

The rest of the article is structured as follows. Section 2 introduces the new methodology, including system design, inverse kinematic modeling, static analysis of cable tensions, and layout optimization. In Section 3, workspace optimization for various CPM configurations is discussed, showing the relationship between workspace size and stiffness. Section 4 provides a discussion of the findings, their broader implications in robotics, and the methodological contributions of the present study.

2. Methodology

This section details the methodology proposed to develop, model, and optimize CPMs for underwater use. The methodology covers system design, kinematic modeling, static analysis, and optimization techniques in the subsections that follow.

2.1. System overview and design

The proposed design involves an end effector operating in deep-sea conditions, connected to surface ships via cables. Motors positioned on the ships control these cables. Two configurations are examined: (i) an eight-ship and (ii) a ten-ship setup.

Fig. 1 shows the eight-ship configuration, designed for precise manipulation and data acquisition in deep-sea environments. Specifically, this figure illustrates the spatial arrangement of the eight-cable system of the CPM, showing the layout importance in achieving operational precision.

Fig. 1 facilitates understanding and visualization on how the components of the CPM, such as ships and cables, work together to control the movements of the end effector. Such visualization is important for grasping the dynamic capabilities of the CPM and its applications in deep-sea tasks. The platform dimensions are $m = 4$ m (length), $n = 5$ m (width), and $o = 0.3$ m (height).

The platform can perform translational and rotational movements, controlled through cable adjustments and ship movements in the (x, y, z)-axes. Each ship is capable of moving within a circular trajectory with a radius of 50 m. To enhance the system stability, especially against sea wave forces, the operational depth of the system is carefully considered. This is represented by the height dimension h shown in Fig. 1, which specifies the vertical distance between the sea surface and the operational depth of the CPM. Selecting an appropriate value for h is crucial for ensuring that the system remains stable under varying sea conditions and at the intended operational depth.

2.2. Inverse kinematic modeling

For the CPM, position and velocity analyses are performed using inverse kinematics. The configuration of the CPM, as shown in Fig. 1, uses eight cables. Position analysis is conducted to determine the lengths of these cables, considering both the position of the manipulator and the locations of the ships.

For the kinematic modeling of the system, the lengths of each of the eight cables collectively determine the positioning of the platform at a desired location and orientation. Then, the cable lengths are calculated as

$$L_1^2 = \left(p_x + (\mathrm{c}(\phi_1)\mathrm{c}(\theta_1))\frac{m}{2} - (\mathrm{c}(\phi_1)\mathrm{s}(\theta_1)\mathrm{s}(\psi_1) - \mathrm{s}(\phi_1)\mathrm{c}(\psi_1))\frac{n}{4} \right.$$

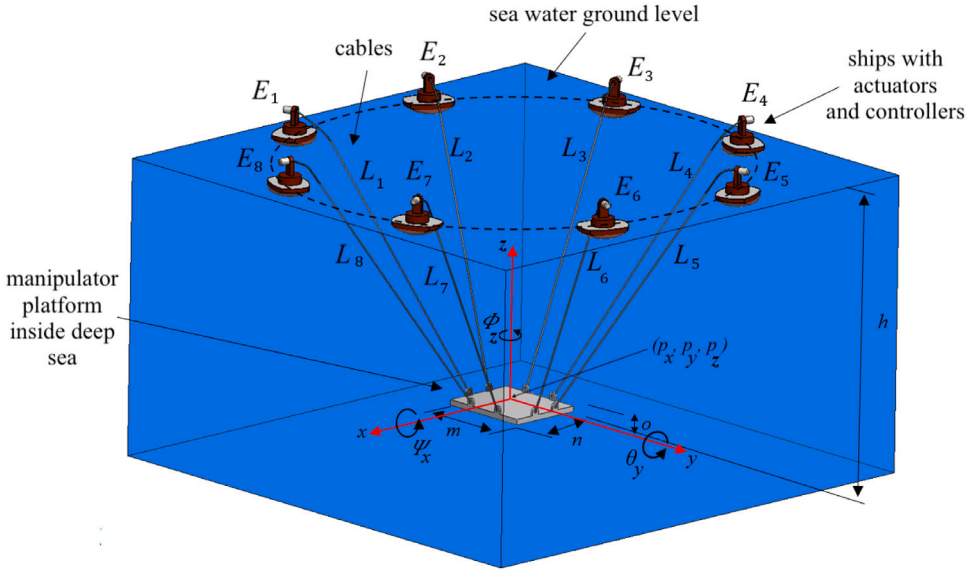

Fig. 1. Schematic illustration depicting the layout of the CPM with eight cables, where m, n, and o are the length, width, and height of the platform, respectively; $E_i = (e_{1i}, e_{2i}, e_{3i})$ are the (x, y, z)-axes coordinates and L_i denotes the length of the cable connected to ship i, for $i = 1, \ldots, 8$. The height dimension h is the vertical distance between the sea surface and the operational depth of the CPM.

$$
\begin{aligned}
L_2^2 = {} & \Big(p_x + (\mathrm{c}(\phi_2)\mathrm{c}(\theta_2))\frac{m}{4} - (\mathrm{c}(\phi_2)\mathrm{s}(\theta_2)\mathrm{s}(\psi_2) - \mathrm{s}(\phi_2)\mathrm{c}(\psi_2))\frac{n}{2} \\
& + (\mathrm{c}(\phi_2)\mathrm{s}(\theta_2)\mathrm{c}(\psi_2) + \mathrm{s}(\phi_2)\mathrm{s}(\psi_2))\frac{o}{2} - e_{12} \Big)^2 \\
& + \Big(p_y + (\mathrm{s}(\phi_2)\mathrm{c}(\theta_2))\frac{m}{4} - (\mathrm{s}(\phi_2)\mathrm{s}(\theta_2)\mathrm{s}(\psi_2) + \mathrm{c}(\phi_2)\mathrm{c}(\psi_2))\frac{n}{2} \\
& + (\mathrm{s}(\phi_2)\mathrm{s}(\theta_2)\mathrm{c}(\psi_2) - \mathrm{c}(\phi_2)\mathrm{s}(\psi_2))\frac{o}{2} - e_{32} \Big)^2 \\
& + \Big(p_z - (\mathrm{s}(\theta_2))\frac{m}{4} - (\mathrm{c}(\phi_2)\mathrm{s}(\psi_2))\frac{n}{2} + (\mathrm{c}(\phi_2)\mathrm{c}(\psi_2))\frac{o}{2} - e_{22} \Big)^2, \qquad (2)
\end{aligned}
$$

$$
\begin{aligned}
L_3^2 = {} & \Big(p_x - (\mathrm{c}(\phi_3)\mathrm{c}(\theta_3))\frac{m}{4} - (\mathrm{c}(\phi_3)\mathrm{s}(\theta_3)\mathrm{s}(\psi_3) - \mathrm{s}(\phi_3)\mathrm{c}(\psi_3))\frac{n}{2} \\
& + (\mathrm{c}(\phi_3)\mathrm{s}(\theta_3)\mathrm{c}(\psi_3) + \mathrm{s}(\phi_3)\mathrm{s}(\psi_3))\frac{o}{2} - e_{13} \Big)^2 \\
& + \Big(p_y - (\mathrm{s}(\phi_3)\mathrm{c}(\theta_3))\frac{m}{4} - (\mathrm{s}(\phi_3)\mathrm{s}(\theta_3)\mathrm{s}(\psi_3) + \mathrm{c}(\phi_3)\mathrm{c}(\psi_3))\frac{n}{2} \\
& + (\mathrm{s}(\phi_3)\mathrm{s}(\theta_3)\mathrm{c}(\psi_3) - \mathrm{c}(\phi_3)\mathrm{s}(\psi_3))\frac{o}{2} - e_{33} \Big)^2 \\
& + \Big(p_z + (\mathrm{s}(\theta_3))\frac{m}{4} - (\mathrm{c}(\phi_3)\mathrm{s}(\psi_3))\frac{n}{2} + (\mathrm{c}(\phi_3)\mathrm{c}(\psi_3))\frac{o}{2} - e_{23} \Big)^2, \qquad (3)
\end{aligned}
$$

$$
\begin{aligned}
L_4^2 = {} & \Big(p_x + (\mathrm{c}(\phi_4)\mathrm{c}(\theta_4))\frac{m}{2} + (\mathrm{c}(\phi_4)\mathrm{s}(\theta_4)\mathrm{s}(\psi_4) - \mathrm{s}(\phi_4)\mathrm{c}(\psi_4))\frac{n}{4} \\
& + (\mathrm{c}(\phi_4)\mathrm{s}(\theta_4)\mathrm{c}(\psi_4) + \mathrm{s}(\phi_4)\mathrm{s}(\psi_4))\frac{o}{2} - e_{14} \Big)^2 \\
& + \Big(p_y - (\mathrm{s}(\phi_4)\mathrm{c}(\theta_4))\frac{m}{2} + (\mathrm{s}(\phi_4)\mathrm{s}(\theta_4)\mathrm{s}(\psi_4) + \mathrm{c}(\phi_4)\mathrm{c}(\psi_4))\frac{n}{4} \\
& + (\mathrm{s}(\phi_4)\mathrm{s}(\theta_4)\mathrm{c}(\psi_4) - \mathrm{c}(\phi_4)\mathrm{s}(\psi_4))\frac{o}{2} - e_{34} \Big)^2 \\
& + \Big(p_z + (-\mathrm{s}(\theta_4))\frac{m}{2} + (\mathrm{c}(\phi_4)\mathrm{s}(\psi_4))\frac{n}{4} + (\mathrm{c}(\phi_4)\mathrm{c}(\psi_4))\frac{o}{2} - e_{24} \Big)^2, \qquad (4)
\end{aligned}
$$

$$
\begin{aligned}
L_5^2 = {} & \Big(p_x - (\mathrm{c}(\phi_5)\mathrm{c}(\theta_5))\frac{m}{2} + (\mathrm{c}(\phi_5)\mathrm{s}(\theta_5)\mathrm{s}(\psi_5) - \mathrm{s}(\phi_5)\mathrm{c}(\psi_5))\frac{n}{4} \\
& + (\mathrm{c}(\phi_5)\mathrm{s}(\theta_5)\mathrm{c}(\psi_5) + \mathrm{s}(\phi_5)\mathrm{s}(\psi_5))\frac{o}{2} - e_{15} \Big)^2 \\
& + \Big(p_y - (\mathrm{s}(\phi_5)\mathrm{c}(\theta_5))\frac{m}{2} + (\mathrm{s}(\phi_5)\mathrm{s}(\theta_5)\mathrm{s}(\psi_5) + \mathrm{c}(\phi_5)\mathrm{c}(\psi_5))\frac{n}{4} \\
& + (\mathrm{s}(\phi_5)\mathrm{s}(\theta_5)\mathrm{c}(\psi_5) - \mathrm{c}(\phi_5)\mathrm{s}(\psi_5))\frac{o}{2} - e_{35} \Big)^2 \\
& + \Big(p_z + (\mathrm{s}(\theta_5))\frac{m}{2} + (\mathrm{c}(\phi_5)\mathrm{s}(\psi_5))\frac{n}{4} + (\mathrm{c}(\phi_5)\mathrm{c}(\psi_5))\frac{o}{2} - e_{25} \Big)^2, \qquad (5)
\end{aligned}
$$

$$
\begin{aligned}
L_6^2 = {} & \Big(p_x - (\mathrm{c}(\phi_6)\mathrm{c}(\theta_6))\frac{m}{4} + (\mathrm{c}(\phi_6)\mathrm{s}(\theta_6)\mathrm{s}(\psi_6) - \mathrm{s}(\phi_6)\mathrm{c}(\psi_6))\frac{n}{2} \\
& + (\mathrm{c}(\phi_6)\mathrm{s}(\theta_6)\mathrm{c}(\psi_6) + \mathrm{s}(\phi_6)\mathrm{s}(\psi_6))\frac{o}{2} - e_{16} \Big)^2 \\
& + \Big(p_y - (\mathrm{s}(\phi_6)\mathrm{c}(\theta_6))\frac{m}{4} + (\mathrm{s}(\phi_6)\mathrm{s}(\theta_6)\mathrm{s}(\psi_6) + \mathrm{c}(\phi_6)\mathrm{c}(\psi_6))\frac{n}{2} \\
& + (\mathrm{s}(\phi_6)\mathrm{s}(\theta_6)\mathrm{c}(\psi_6) - \mathrm{c}(\phi_6)\mathrm{s}(\psi_6))\frac{o}{2} - e_{36} \Big)^2 \\
& + \Big(p_z + (\mathrm{s}(\theta_6))\frac{m}{4} - (\mathrm{c}(\phi_6)\mathrm{s}(\psi_6))\frac{n}{2} + (\mathrm{c}(\phi_6)\mathrm{c}(\psi_6))\frac{o}{2} - e_{26} \Big)^2, \qquad (6)
\end{aligned}
$$

$$
\begin{aligned}
L_7^2 = {} & \Big(p_x + (\mathrm{c}(\phi_7)\mathrm{c}(\theta_7))\frac{m}{4} + (\mathrm{c}(\phi_7)\mathrm{s}(\theta_7)\mathrm{s}(\psi_7) - \mathrm{s}(\phi_7)\mathrm{c}(\psi_7))\frac{n}{2} \\
& + (\mathrm{c}(\phi_7)\mathrm{s}(\theta_7)\mathrm{c}(\psi_7) + \mathrm{s}(\phi_7)\mathrm{s}(\psi_7))\frac{o}{2} - e_{17} \Big)^2 \\
& + \Big(p_y + (\mathrm{s}(\phi_7)\mathrm{c}(\theta_7))\frac{m}{4} + (\mathrm{s}(\phi_7)\mathrm{s}(\theta_7)\mathrm{s}(\psi_7) + \mathrm{c}(\phi_7)\mathrm{c}(\psi_7))\frac{n}{2} \\
& + (\mathrm{s}(\phi_7)\mathrm{s}(\theta_7)\mathrm{c}(\psi_7) - \mathrm{c}(\phi_7)\mathrm{s}(\psi_7))\frac{o}{2} - e_{37} \Big)^2 \\
& + \Big(p_z + (-\mathrm{s}(\theta_7))\frac{m}{4} + (\mathrm{c}(\phi_7)\mathrm{s}(\psi_7))\frac{n}{2} + (\mathrm{c}(\phi_7)\mathrm{c}(\psi_7))\frac{o}{2} - e_{27} \Big)^2, \qquad (7)
\end{aligned}
$$

$$
\begin{aligned}
L_8^2 = {} & \Big(p_x + (\mathrm{c}(\phi_8)\mathrm{c}(\theta_8))\frac{m}{2} + (\mathrm{c}(\phi_8)\mathrm{s}(\theta_8)\mathrm{s}(\psi_8) - \mathrm{s}(\phi_8)\mathrm{c}(\psi_8))\frac{n}{2} \\
& + (\mathrm{c}(\phi_8)\mathrm{s}(\theta_8)\mathrm{c}(\psi_8) + \mathrm{s}(\phi_8)\mathrm{s}(\psi_8))\frac{o}{2} - e_{18} \Big)^2 \\
& + \Big(p_y + (\mathrm{s}(\phi_8)\mathrm{c}(\theta_8))\frac{m}{2} - (\mathrm{s}(\phi_8)\mathrm{s}(\theta_8)\mathrm{s}(\psi_8) + \mathrm{c}(\phi_8)\mathrm{c}(\psi_8))\frac{n}{2} \\
& + (\mathrm{s}(\phi_8)\mathrm{s}(\theta_8)\mathrm{c}(\psi_8) - \mathrm{c}(\phi_8)\mathrm{s}(\psi_8))\frac{o}{2} - e_{38} \Big)^2 \\
& + \Big(p_z + (-\mathrm{s}(\theta_8))\frac{m}{2} + (\mathrm{c}(\phi_8)\mathrm{s}(\psi_8))\frac{n}{2} + (\mathrm{c}(\phi_8)\mathrm{c}(\psi_8))\frac{o}{2} - e_{28} \Big)^2, \qquad (8)
\end{aligned}
$$

where p_x, p_y, and p_z denote the positions of the manipulator along the x-axis, y-axis, and z-axis, respectively, indicating the precise location of the manipulator geometric center on the platform, which theoretically serves as the anchor point from which all cables extend to the ships; ψ_i, θ_i, and ϕ_i represent the angles of rotation around the x-axis, y-axis, and z-axis, respectively, for each cable i, where $i = 1, \ldots, 8$. These angles are known as Roll–Pitch–Yaw angles varying to adjust the platform orientation and position in the deep-sea environment. The parameters e_{1i}, e_{2i}, and e_{3i} represent the coordinates of the attachment points of cable i on the ship, within a stable coordinate framework. To simplify Eqs. (1) to (8), and enhance their readability, the notation c is used to denote the cosine function and s for the sine function. For example, $\mathrm{c}(\phi_i)$ and $\mathrm{s}(\phi_i)$ represent the cosine and sine of angle ϕ_i, respectively. This notation for trigonometric functions and subscripted angles is applied consistently throughout the whole article.

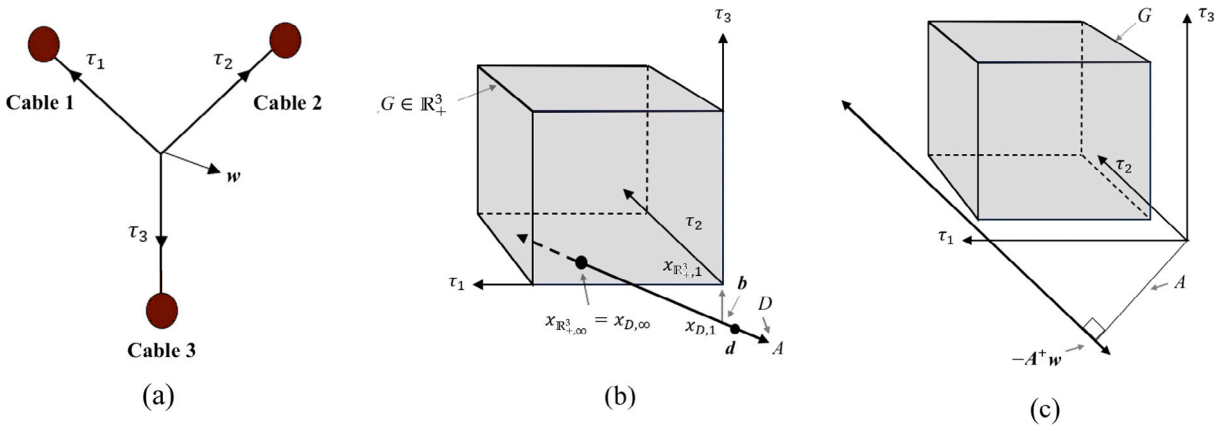

Fig. 2. Plots of (a) planar translational CPM with three cables; (b) feasible solution space where sets A and G intersect –Case 1–; and (c) scenario depicting the absence of feasible solutions due to no intersection between sets A and G –Case 2–, where τ_i represents the tension in cable i, w is the wrench applied to the manipulator, x_S is a convergence point at a generic set S, D is a line segment with its directional vector d and b is a perpendicular vector to d.

2.3. Static analysis: Bounded cable tensions

The operation of the CPM involves application of forces and moments by the end effector on external environment. To ensure stable and controlled movement, each cable in the CPM system is maintained at a predetermined tension level. This operation allows for a direct correlation between applied force on the mobile platform and tensions in the cables. The relationship between the applied wrench (force and moment) and the cable tensions is given by

$$\boldsymbol{w} = \begin{bmatrix} \boldsymbol{f} \\ \boldsymbol{m} \end{bmatrix} = -\boldsymbol{A}\boldsymbol{\tau}, \tag{9}$$

where $\boldsymbol{w}$ represents the wrench vector applied to the manipulator, consisting of the force vector $\boldsymbol{f}$ and the moment vector $\boldsymbol{m}$, whereas the vector $\boldsymbol{\tau}$ represents the tensions in the cables. Matrix $\boldsymbol{A}$ in Eq. (9) is defined as

$$\boldsymbol{A} = \begin{bmatrix} \hat{l}_1 & \dots & \hat{l}_k \\ z_1 \hat{l}_1 & \dots & z_k \hat{l}_k \end{bmatrix},$$

where $\hat{l}_i$ is the unit vector in the direction of cable length L_i and z_i is the vector from the base of the manipulator to the attachment point of cable i in the global reference frame, for $i = 1, \dots, k$. The expression given in Eq. (9) can be expanded as

$$\boldsymbol{\tau} = -\boldsymbol{A}^+\boldsymbol{w} + \boldsymbol{\Omega}\boldsymbol{u}, \tag{10}$$

where $\boldsymbol{A}^+$ represents the pseudo-inverse of matrix $\boldsymbol{A}$, $\boldsymbol{\Omega}$ is the null space of $\boldsymbol{A}$, and $\boldsymbol{u}$ is a vector containing any real numbers. The solution $\boldsymbol{\tau}$ of Eq. (10) is found at the intersection of two convex sets, represented as $\boldsymbol{\tau} \in C \equiv G \cap A$, where set A is defined from the matrix $\boldsymbol{A}$ as

$$A \equiv \{\boldsymbol{\tau} = -\boldsymbol{A}^+\boldsymbol{w} + \boldsymbol{\Omega}\boldsymbol{u}\}. \tag{11}$$

Before proceeding, it is necessary to define a key geometric concept used in this analysis. An orthant in geometry is a generalization of a quadrant in two dimensions or an octant in three dimensions, representing one of the 2^k parts into which a k-dimensional space is divided by mutually perpendicular planes. This concept is crucial for understanding set G, which is defined as an multidimensional orthant. Specifically, set G is characterized by the cable tension constraints and is formulated as

$$G \equiv \{\|\boldsymbol{\tau}_{i_{\min}}\| \leq \|\boldsymbol{\tau}_i\|, \forall\, i = 1, \dots, k\}, \tag{12}$$

where, for each cable i, tension $\|\boldsymbol{\tau}_i\|$ is bounded from below by $\|\boldsymbol{\tau}_{i_{\min}}\|$, being the minimum allowable tension, and it does not have an upper limit.

The full formulation stated above is essential for categorizing the operations of the CPM into two our distinct cases: Case 1 and Case 2.

In Case 1, the intersection, set C say, is formed by the intersection of sets G and A. Set G, defined in Eq. (12), represents the cable tension constraints in an multidimensional orthant. Set A, defined in Eq. (11), states the system constraints in terms of cable tensions. The non-empty intersection of G and A in set C indicates the presence of at least one feasible solution, showing an overlap in the operational constraints of the CPM and the allowable cable tension ranges.

Fig. 2 provides a visual representation of these theoretical concepts. In Fig. 2a, a planar translational CPM with three cables is depicted, with each cable representing a unique degree of freedom. The vectors $\boldsymbol{\tau}_1$, $\boldsymbol{\tau}_2$, and $\boldsymbol{\tau}_3$ correspond to the tensions in cables 1, 2, and 3, respectively, defining the CPM operational space. Fig. 2b (Case 1) illustrates the scenario where the affine set A intersects with orthant G, depicted as a parallelepiped, in $\mathbb{R}^3_+$ space, suggesting multiple feasible solutions for cable tensions. This is further exemplified by set D, represented as a line segment with the directional vector $\boldsymbol{d}$, which intersects this space. The vector $\boldsymbol{b}$, perpendicular to $\boldsymbol{d}$, illustrates the projection of this intersection point, indicating feasible solutions.

Conversely, Case 2 arises when the intersection set C is empty, suggesting that there are no feasible solutions that satisfy the system constraints. This scenario is visually represented in Fig. 2c. In this figure, orthant G, depicted as a parallelepiped, represents the space of feasible cable tensions. The affine set A, mathematically defined as the result of applying the pseudo-inverse $-\boldsymbol{A}^+$ to the wrench vector $\boldsymbol{w}$, is depicted as being perpendicular to the vector resulting from $-\boldsymbol{A}^+\boldsymbol{w}$. Crucially, this line segment (representing A) does not intersect with the parallelepiped G, the latter of which delineates the permissible range of cable tensions. The absence of intersection between A and G in this visual representation signifies that the system constraints, as defined by A, cannot be satisfied within the allowable tension ranges of the cables (represented by G). Therefore, in this scenario, there are no feasible solutions for the cable tensions that meet the system requirements. The analysis presented in these figures is integral to applying the Dykstra algorithm for finding the minimum-2-norm solution for cable tensions in CPMs.

Inverse kinematic modeling of CPMs involves assumptions and simplifications that can introduce errors. These errors may include the idealization of cable behavior and neglecting factors such as cable elasticity and friction. While these assumptions simplify the model and make calculations feasible, they can lead to deviations from real-world behavior. To mitigate the effects of these errors, the models are validated against a set of controlled simulations, ensuring that the discrepancies remain within acceptable margins for the intended applications.

2.4. Adaptation of the Dykstra algorithm for CPMs

The Dykstra algorithm (Dykstra, 1983) is a recursive method designed to identify a point at the intersection of multiple convex sets. This algorithm is helpful for optimization and computation of mathematical problems where constraints are often represented as intersections of convex sets.

Adaptation of the Dykstra algorithm to the specific context of CPMs is a contribution of the present study. This algorithm is adapted for an iterative computation of cable tension solutions that concurrently satisfy all convex constraints. The algorithm projects a point iteratively onto convex sets, starting with set A, as defined in Eq. (11), which embodies the affine transformation constraints of the system, and subsequently onto set G, a k-dimensional orthant that defines the tension limits for each cable, as outlined in Eq. (12). This iterative correction process of the algorithm considers the error from the previous projection, ensuring that the sequence of points progresses towards the intersection within the convex sets A and G, assuming that such an intersection exists. This process is crucial for the present study of CPMs, where dynamic requirements necessitate adaptations of the algorithm. The customized selection of sets A and G aligns with the operational dynamics and tension limits of CPMs, enhancing both operational stability and precision.

Parameters for the Dykstra algorithm, such as the initial point t_0, maximum iterations N, and tolerances ϵ_x and ϵ_y, were chosen to balance operational precision and computational efficiency. The initial point t_0 was determined based on preliminary simulations, offering a feasible starting position within the solution space. The defined maximum iterations N and tolerances ϵ_x and ϵ_y ensure iterative refinement of the solution without overburdening computational resources.

Our application of the Dykstra algorithm presents a novel approach to address the specific challenge of optimizing cable tensions in CPMs. By iteratively projecting a point onto A and G, the algorithm adapts to satisfy all the operational constraints of the CPM system. This approach is not only about finding an intersection point within the sets but also about improving the efficiency and precision of cable tension determination, as evidenced by comparative analyses with traditional optimization methods.

The pseudo-code presented in Algorithm 1 and the flowchart illustrated in Fig. 3 offer a detailed outline of the Dykstra algorithm implementation in the context of cable tension optimization for CPMs. This implementation serves to clarify our methodology and acts as a resource for future applications of the Dykstra algorithm in similar contexts within underwater robotics. The notations used in Algorithm 1 are defined in the next subsection.

Algorithm 1 Dykstra projection algorithm.

Require: Initial point t_0, convex sets A, G, maximum iterations N, and tolerances ϵ_x, ϵ_y
Ensure: $\|\boldsymbol{\tau}_{\min}\|$
for $i = 1$ to N **do**
  $x_A \leftarrow \text{proj}_A(t)$
  $r_A \leftarrow t - x_A$
  $t \leftarrow t + 2r_A$
  $x_G \leftarrow \text{proj}_G(t)$
  $r_G \leftarrow t - x_G$
  $t \leftarrow t + 2r_G$
  if $(\|x_{A,i} - x_{A,i-1}\| + \|x_{G,i} - x_{G,i-1}\| \le \epsilon_x)$ and $(\|y_{A,i} - y_{A,i-1}\| + \|y_{G,i} - y_{G,i-1}\| \le \epsilon_y)$ **then**
    break
  end if
end for
return $\|\boldsymbol{\tau}_{\min}\| = \text{proj}_C(0) = x_{G,\infty} = x_{A,\infty}$

Errors can arise from the choice of initial conditions, setting of algorithmic parameters, and inherent limitations of the algorithm in handling non-linear constraints.

To evaluate the reliability of the algorithm, multiple test cases with known solutions were analyzed, comparing the algorithm outcomes with these benchmarks. Additionally, the impact of varying the initial conditions and algorithmic parameters on the solution accuracy was examined to ensure the robustness of the method.

2.5. Cable tension optimization

The cable tensions derived from Eq. (10) do not necessarily correspond to the minimum tensions required. To identify the minimum-2-norm solution for $\boldsymbol{\tau}$, it is crucial to locate the solution within set C. This set, defined as the intersection of sets A and G in Eqs. (11) and (12), encompasses feasible cable tension configurations. As mentioned, set A is the affine transformation of the system, while G is a k-dimensional orthant specifying the tension limits for each cable.

To determine the minimum-2-norm solution within C, the Dykstra algorithm is employed. The 2-norm of $\boldsymbol{\tau}$ signifies the shortest Euclidean distance from the origin to a point in C, denoted as $\|\mathbf{0} - \boldsymbol{\tau}\|$. This point represents the configuration within C with the closest Euclidean distance to the origin. The projection of this minimal distance onto C is mathematically expressed as

$$\|\boldsymbol{\tau}\| = \text{proj}_c(\mathbf{0}) = \arg\min_{\tau \in C} \|\mathbf{0} - \boldsymbol{\tau}\|, \tag{13}$$

where the notation $\text{proj}_C(\mathbf{0})$ used in Eq. (13) indicates the projection of the origin onto the convex set C.

The Dykstra algorithm, as derived from Eq. (13), is utilized to compute $||\boldsymbol{\tau}_{\min}||$. This algorithm is implemented on the manipulator shown in Fig. 1. The process begins at the origin, iteratively projecting a point within the confines of set C. Each iteration involves computing an intermediate point, denoted as $\boldsymbol{x}_i$, which symbolizes the current position in the solution space defined by C. This point $\boldsymbol{x}_i$ is progressively adjusted towards the optimal solution, aligning with the constraints imposed by sets A and G. If set C is non-empty, it is expected that the sequence of vectors $\boldsymbol{x}_j$ will converge to a unique point within C as the number of iterations j increases. This point of convergence is significant, representing the position in C with the least Euclidean distance from the origin, so defining the minimum norm solution for vector $\boldsymbol{\tau}$. At each iteration, the algorithm calculates $\boldsymbol{x}_{A,j} = \text{proj}_A(\boldsymbol{x}_{G,j-1})$ and $\boldsymbol{x}_{G,j} = \text{proj}_G(\boldsymbol{x}_{A,j})$, corresponding to the projections of the point from the previous iteration onto sets A and G, respectively. The process continues until the convergence points $\boldsymbol{x}_{A,\infty}$ and $\boldsymbol{x}_{G,\infty}$ are reached, indicated by minimal changes between successive iterations.

The point of convergence, $\boldsymbol{x}_{G,\infty} = \boldsymbol{x}_{A,\infty}$ namely, is the minimum Euclidean distance from the initial point in set C, which is described by $||\boldsymbol{\tau}_{\min}|| = \text{proj}_C(\mathbf{0}) = \boldsymbol{x}_{G,\infty} = \boldsymbol{x}_{A,\infty}$. In each iteration of the Dykstra algorithm, two key computations are performed: the projection of the current point onto sets A and G. The projection onto set A, denoted as $\text{proj}_A(t)$, is defined by

$$\text{proj}_A(t) = (\boldsymbol{I} - \boldsymbol{A}^+\boldsymbol{A})\boldsymbol{t} - \boldsymbol{A}^+\boldsymbol{w}, \tag{14}$$

where $\boldsymbol{I}$ is the identity matrix and $\boldsymbol{t}$ undergoes projection onto the null space of $\boldsymbol{A}$, followed by a translation due to $-\boldsymbol{A}^+\boldsymbol{w}$. Similarly, the projection onto set G is computed, which adjusts the current point in accordance with the tension limits defined by G. The iterative process continues until the projections $\boldsymbol{x}_{A,j}$ and $\boldsymbol{x}_{G,j}$ converge, leading to the final points $\boldsymbol{x}_{A,\infty}$ and $\boldsymbol{x}_{G,\infty}$.

Analogously, the computation of $\text{proj}_G(\boldsymbol{t})$ can be formulated as $\text{proj}_G(\boldsymbol{t}) = [\bar{t}_1 \ \dots \ \bar{t}_n]$, where

$$\bar{t}_i = \begin{cases} \|\boldsymbol{\tau}_{i_{\min}}\|, & \text{if } t_i \le \|\boldsymbol{\tau}_{i_{\min}}\|; \\ t_i, & \text{if } \|\boldsymbol{\tau}_{i_{\min}}\| \le t_i \le \|\boldsymbol{\tau}_{i_{\max}}\|; \\ \|\boldsymbol{\tau}_{i_{\max}}\|, & \text{if } t_i \ge \|\boldsymbol{\tau}_{i_{\max}}\|; \end{cases} \tag{15}$$

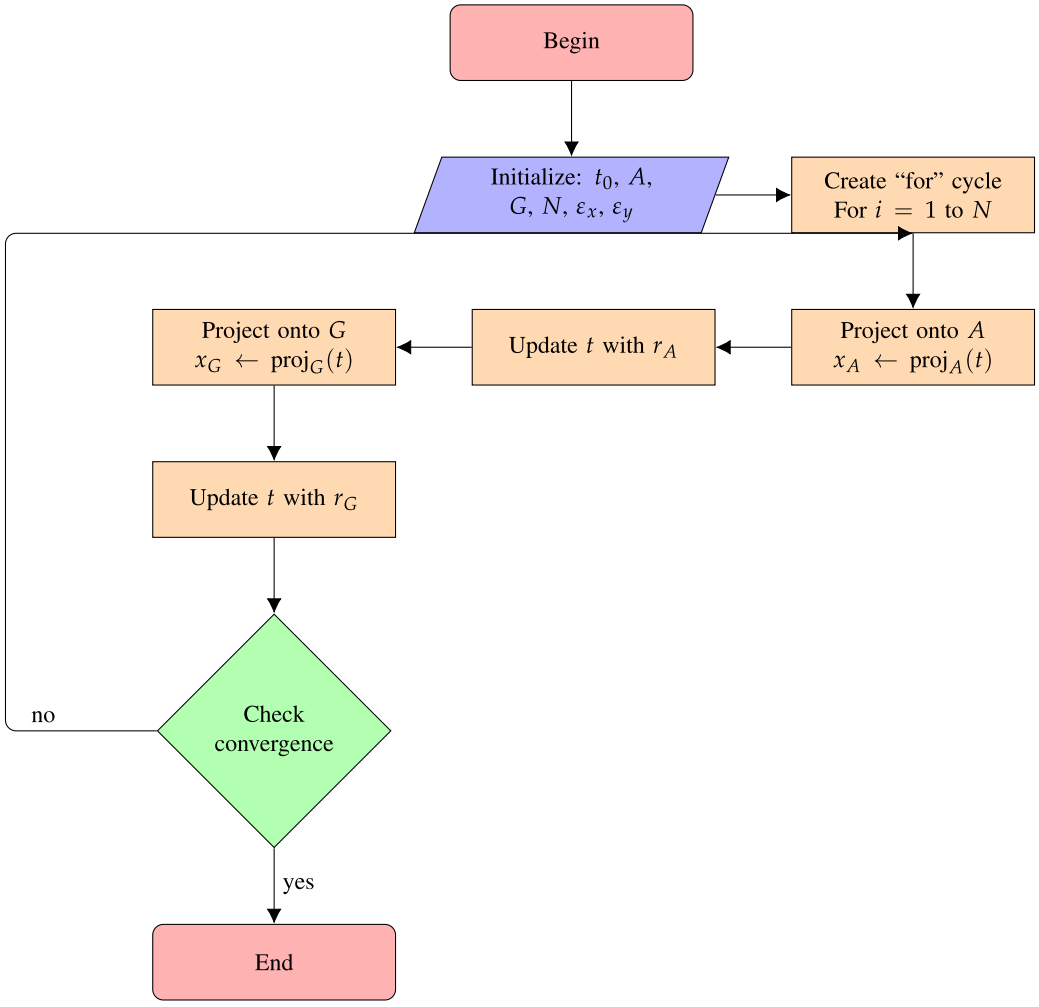

Fig. 3. Flowchart of the Dykstra projection algorithm for CPM tension optimization.

with Eq. (15) adjusting the coordinates $\boldsymbol{t}$ to ensure they fall within the bounds of the orthant G, setting the values of $\bar{t}_i$ in accordance with the predefined tension limits.

In Fig. 2c, where set C lacks intersections, the sequences $x_{k,j}$ diverge towards two distinct points, rather than converging to a single point. In such cases, the Dykstra algorithm determines the feasibility of a solution for $\boldsymbol{\tau}$ exists under the conditions outlined in Eq. (9) with respect to a given force $\boldsymbol{w}$. Specifically, if $\boldsymbol{x}_{G,\infty} = \boldsymbol{x}_{A,\infty}$, then the applied wrench $\boldsymbol{w}$ is considered feasible; otherwise, it is deemed infeasible. As part of the Dykstra algorithm, the convergence of the iterative process is determined using specific tolerances. These tolerances are applied to the changes in the projected points over successive iterations. The criteria for termination are defined by

$$\|\hat{\boldsymbol{x}}_{A,j} - \hat{\boldsymbol{x}}_{A,j-1}\| + \|\hat{\boldsymbol{x}}_{G,j} - \hat{\boldsymbol{x}}_{G,j-1}\| \leq \varepsilon_x,$$

where $\hat{\boldsymbol{x}}_{A,j}$ and $\hat{\boldsymbol{x}}_{G,j}$ are projections onto sets A and G in ith iteration, respectively. Also, the algorithm checks the condition

$$\|\hat{\boldsymbol{y}}_{A,j} - \hat{\boldsymbol{y}}_{A,j-1}\| + \|\hat{\boldsymbol{y}}_{G,j} - \hat{\boldsymbol{y}}_{G,j-1}\| \leq \varepsilon_y,$$

where $\hat{\boldsymbol{y}}_{A,j}$ and $\hat{\boldsymbol{y}}_{G,j}$ are normalizations of $\hat{\boldsymbol{x}}_{A,j}$ and $\hat{\boldsymbol{x}}_{G,j}$, respectively. These conditions with tolerances ε_x and ε_y state the change level between iterations for the algorithm to be considered as converging.

The static analysis of cable tensions in CPMs is subject to uncertainties related to material properties and environmental conditions. Variations in cable stiffness, unaccounted external forces, and measurement inaccuracies can affect the precision of the tension calculations. To address these potential errors, a sensitivity analysis was conducted, examining how variations in cable properties and external conditions influence the tension outcomes. This analysis helps in understanding the robustness of the manipulator design under varying operational scenarios.

2.6. Layout optimization

After optimizing the cable tensions, the workspace of the CPM is outlined to facilitate layout optimization. This workspace involves determining the optimal positions for the ships as illustrated in Fig. 1. Here, the primary aim is to maximize the manipulator workspace, which encompasses all achievable poses of the manipulator while meeting specific conditions. Hence, the optimal positions of the ships are determined not only to maximize the workspace volume but also to consider the manipulator stiffness and natural frequencies.

Next, maximization of the workspace volume is discussed. The main objective in this phase is to pinpoint the optimal positions for the ships, enabling the manipulator to cover the maximum possible volume within its workspace. For a cable-driven manipulator, the workspace is characterized by the set of poses that the manipulator can feasibly achieve, which depends on:

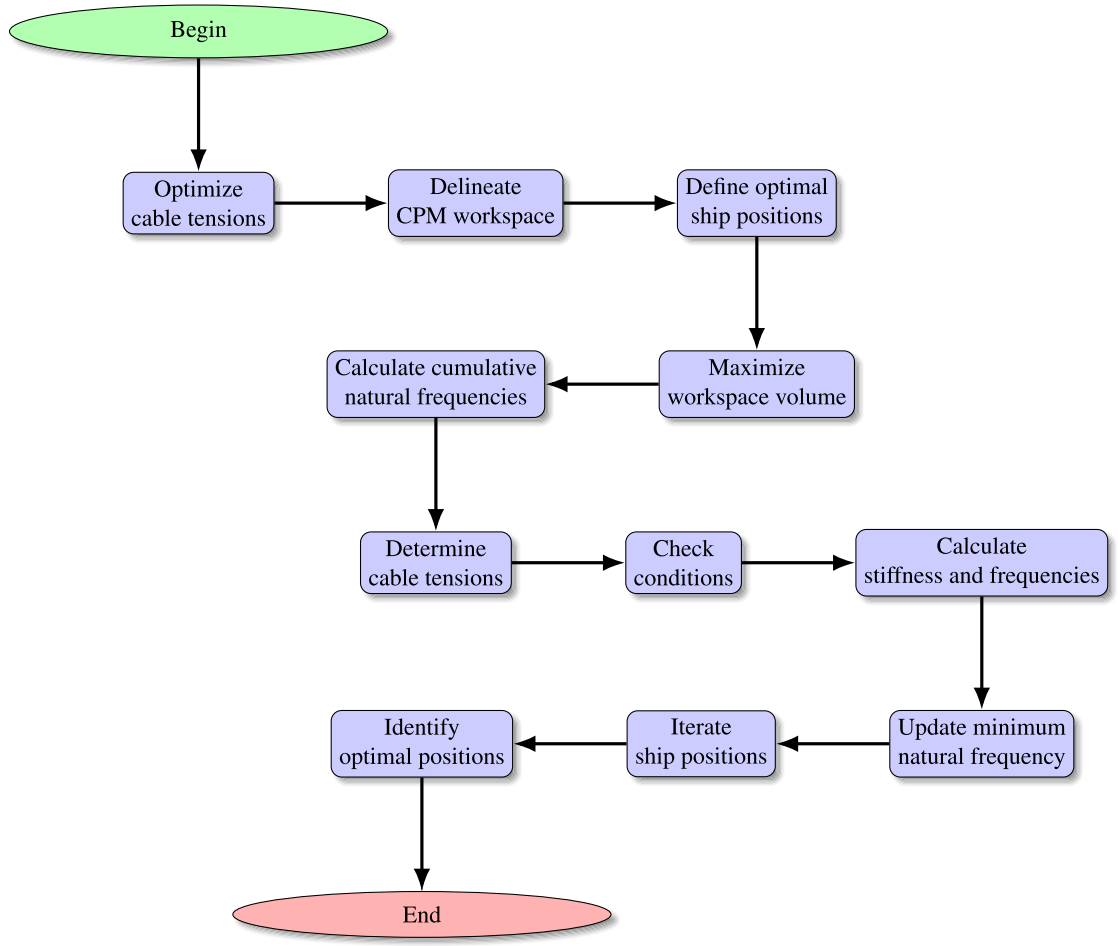

Fig. 4. Flowchart of the layout optimization process.

- Maintaining positive tensions in the cables, meaning $\|\boldsymbol{\tau}_i\| > 0$, for all $i = 1, \ldots, k$.
- Ensuring the manipulator avoids singular conditions, which occur when the rank of the manipulator Jacobian matrix does not equal its degrees of freedom. Avoiding such conditions is crucial for the effective and safe operation of the manipulator.

Now, the maximum stiffness in the workspace is stated. To optimize both translational and rotational stiffness, which have distinct physical units, the concept of natural frequencies is employed. Here, the objective is to increase the stiffness of the system, achieved by elevating the lowest natural frequency. This frequency reflects the system stiffness, with higher values indicating greater stiffness.

Our approach determines the optimal ship positions – a key factor influencing the manipulator stiffness. This entails maximizing the lowest natural frequencies across various manipulator orientations, representing the minimum natural frequency observed at a pose of the manipulator. This maximization is the core to enhance stiffness. To identify these optimal ship positions that fortify the system stiffness, a comprehensive analysis is conducted. Then, the minimum natural frequencies are aggregated across all end-effector poses that maintain positive cable tensions. This exhaustive analysis enables us to precisely pinpoint the ship positions that collectively enhance the manipulator overall stiffness.

The approach commences calculating the sum of the minimum natural frequencies across the entire workspace for a specific set of ship positions. For each manipulator configuration and ship placement, cable tensions are computed using Eqs. (1) to (8) and (10), in conjunction with the Dykstra algorithm outlined in Eq. (13). The algorithm subsequently verifies the mentioned two critical conditions: ensuring positive cable tensions and confirming that the rank of the manipulator Jacobian matrix matches its degrees of freedom. Our approach facilitates the evaluation of the manipulator stiffness under various configurations and enables one to identify ship positions that maximize stiffness across the workspace.

Upon validation, the algorithm calculates the stiffness and natural frequencies of the manipulator. With its inherent degrees of freedom, the manipulator exhibits distinct natural frequencies for each pose. The minimum frequency is continuously updated, aggregating the values from all poses of the manipulator. This leads to the summation of the minimum natural frequency across all poses, providing a measure of stiffness throughout the workspace.

The proposed methodology iteratively evaluates various ship positions, repeating the stiffness accumulation process with each iteration. This methodological approach ultimately pinpoints the ship positions that achieve the maximum summation of the minimum natural frequencies, so maximizing the manipulator stiffness. To illustrate the sequential steps involved in the layout optimization process, refer to the flowchart shown in Fig. 4.

3. Results

This section presents the findings derived from the methodology proposed, elucidating the optimization results for the different configurations of CPMs in terms of workspace and stiffness. To ensure clarity and replicability of these findings, the following subsection details the software and simulation settings used in the study.

3.1. Software and simulation configuration

The simulations were conducted using the software MATLAB R2022a, known for its advanced computational capabilities and extensive toolbox support, making it ideal for complex numerical analyses in robotic simulations. The following simulation settings were employed:

[Computational environment] Simulations were run on a MacBook Pro computer with an Intel Core i9 processor, 32 GB RAM, operating on macOS Big Sur.

[Model parameters] These parameters of the cable-based manipulator included cable lengths, tensions, positions, and weight of the manipulator, whose parameters were essential for accurately replicating the physical behavior of the manipulator system.

[Resolution/accuracy settings] Simulations were executed with a time step of 0.01 s and a convergence tolerance of 10^{-6}, ensuring precise and reliable results.

[Iterative procedures] The Dykstra algorithm implementation involved 1000 iterations with a stopping criterion based on the convergence of the solution, ensuring robustness in finding feasible cable tension solutions.

[Workspace analysis] The workspace optimization was conducted in MATLAB optimization toolbox. The focus was on varying the manipulator pose and calculating the workspace coverage, aiming to maximize the operational area of the manipulator.

These settings were selected to balance computational efficiency with the accuracy necessary for meaningful and reliable results in the study of the manipulator workspace and stiffness characteristics.

3.2. Workspace optimization for the eight-cable manipulator

The inverse kinematics of the eight-cable manipulator are computed utilizing Eqs. (1) to (8) and (10). The Dykstra algorithm, as applied earlier, optimizes cable tensions $\boldsymbol{\tau}$ and assesses the feasibility of these tensions for a specified wrench $\boldsymbol{w}$ as described in Eq. (9).

The inclusion of each manipulator pose in the workspace is contingent upon two critical conditions: (i) $\|\boldsymbol{\tau}_i\| > 0$ for all cables $i = 1, \ldots, k$, with k being the number of cables; and (ii) $\text{rank}(\boldsymbol{J}) = k$, where $\boldsymbol{J}$ is the manipulator Jacobian matrix. The first condition ensures that all cables maintain positive tension, which is essential for the stable operation of the cable-driven manipulator, where the second condition guarantees that the manipulator avoids singular positions, ensuring full control over its movements. These conditions together define the operational limits within which the manipulator can effectively work. This sequence is systematically repeated for each pose of the manipulator to map out the entire workspace. The iterative procedure is executed across various combinations of ship positions.

After ensuring conditions (i) and (ii) above, the next phase focuses on maximizing the workspace volume. This is achieved by finding the optimal positions for the ships that control the manipulator, as illustrated in Fig. 1. Optimal ship positions not only aim to maximize the workspace volume but also consider factors like manipulator stiffness and natural frequencies, linking back to the earlier discussion on cable tension optimization. An aerial view of the optimized ship positions, leading to the most extensive workspace coverage, is shown in Fig. 5. Different ship configurations are analyzed for their impact on the manipulator accessible workspace. Location # 1 in Fig. 5 allows the manipulator to access 2428 distinct poses, the highest among the configurations tested. Subsequent configurations show a gradual decrease in the count of unique accessible poses.

The analysis, focusing on Location # 1, identifies feasible manipulator poses within the constraints. The workspace is defined by maintaining constant orientation angles ψ_x, θ_y, and ϕ_z, and then incrementally varying them to observe changes in the workspace. The angles range from [0, 70] for ψ_x, [0, 65] for θ_y, to [0, 30] for ϕ_z. In the case of Location # 2, the manipulator can access 2317 unique poses within its workspace. This continues for Locations # 3, # 4, and # 5, where the count of distinct poses incrementally diminishes to 2301, 2297, and 2231, respectively. Hence, upon aiming to find the ship positions that maximize the workspace of the manipulator, Location # 1 in Fig. 5 emerges as the optimal choice.

Having established the optimal ship configurations, we now turn our attention to how the manipulator orientation angles ψ_x, θ_y, and ϕ_z influence its operational workspace. This aspect is critical for optimizing the manipulator performance across various tasks. The effect of modulating ϕ_x on the manipulator poses is illustrated in Fig. 6.

We observe an expansion of the workspace ψ_x increases up to a critical point of $\psi_x = 60°$. Beyond this angle, the workspace begins to contract, reducing when ψ_x reaches or exceeds 75°.

The mentioned expansion followed by contraction across the range of [0, 70] degrees for ψ_x provides insights into the manipulator operational limits under different orientation settings. Similarly, variations in θ_y, while maintaining ψ_x and ϕ_z constant, lead to changes in the workspace. This expands up to $\theta_y = 40°$ and then undergoes a gradual reduction as θ_y approaches its upper limit of 65°. These observations are graphically represented in Fig. 7, offering a visual depiction of the workspace alterations when changing the values of θ_y.

Lastly, the workspace is influenced by adjustments in ϕ_z. Initially, increasing ϕ_z results in an enlarged workspace. However, akin to the patterns for ψ_x and θ_y, the workspace diminishes in both size and shape when increasing ϕ_z. Fig. 8 shows contraction of the workspace in the x-y plane when varying the angle θ_y. This figure highlights the dynamic nature of the workspace, underscoring the impact of angular orientation on the manipulator operational space.

3.3. Workspace and stiffness optimization

We extend our study to the workspace optimization of a ten-cable manipulator from the eight-cable configuration. While the ten-cable manipulator shares mechanical characteristics with the eight-cable system, it offers unique advantages in workspace coverage. Employing the algorithm of Fig. 4, we determine the optimal ship positions for the ten-cable system. Results, illustrated in Fig. 9, provide a comparison against the eight-cable configuration. Here, the top five optimal positions for a ten-cable manipulator are identified, emphasizing criteria that maximize its workspace.

In evaluating various ship configurations, we maximize the operational area of the manipulator. The most effective arrangement, as shown in Location #1 in Fig. 9, achieves 3823 distinct poses, surpassing the eight-cable manipulator workspace. This underscores the benefits of increasing the number of cables. Location #2 yields a slightly smaller workspace of 3717 points, with a consistent decrease observed in Locations #3 to #5. This trend demonstrates the impact of cable count on expanding the manipulator workspace.

Subsequently, we shift our focus to the stiffness optimization of the eight-cable manipulator. Analyzing the system performance through the lowest natural frequencies associated with various ship positions, as shown in Fig. 10, highlights the top configurations enhancing system stiffness.

Similarly to the ten-cable manipulator, we identify the optimal ship positions for maximizing stiffness. Results depicted in Fig. 11 indicate the most effective configurations for achieving peak stiffness. Notably, the highest cumulative natural frequency, observed in Location #1, equates to 3823, indicating superior stiffness. This is in contrast to the diminishing values observed in subsequent ship positions, reflecting a decrease in overall system stiffness and structural rigidity.

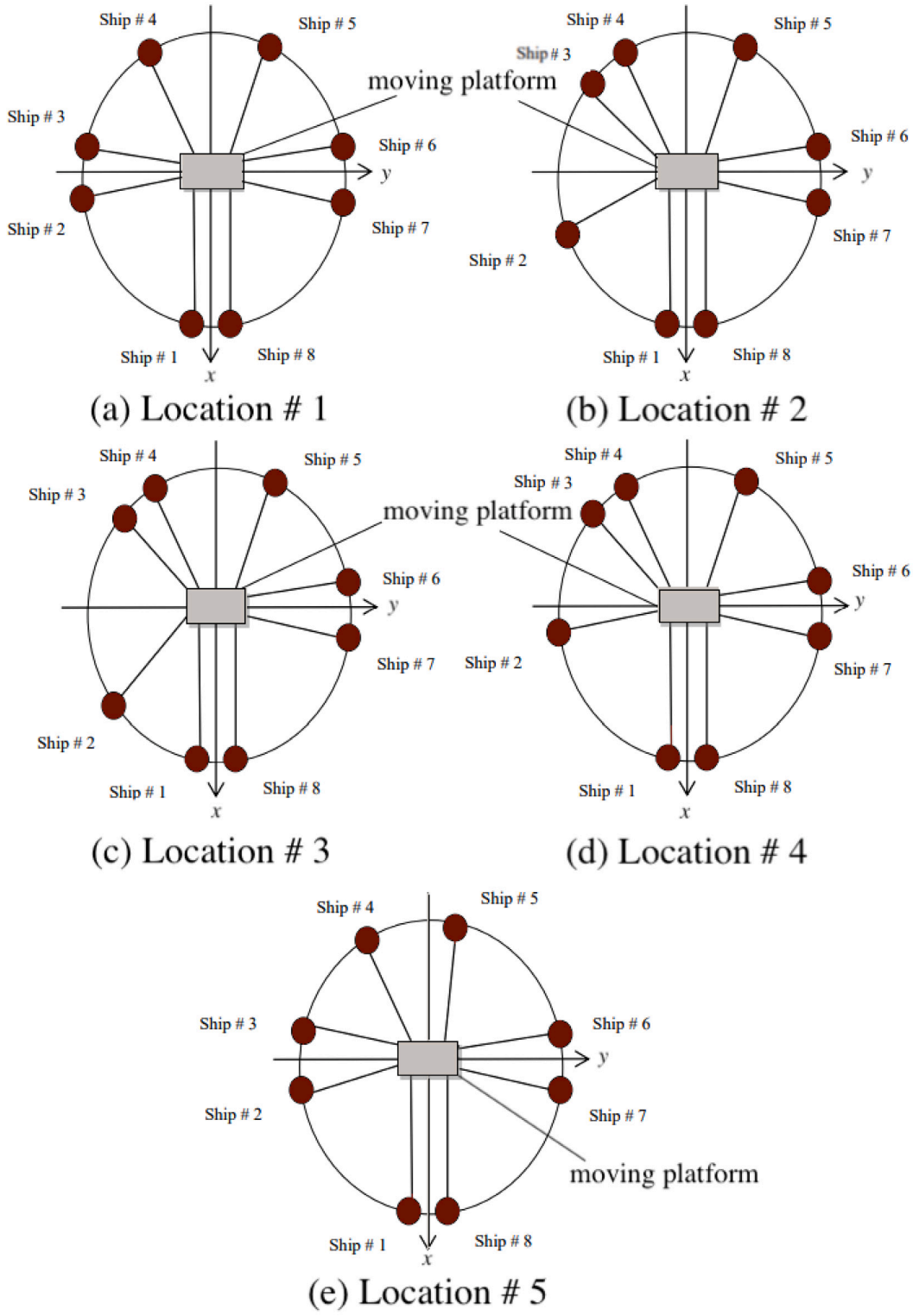

Fig. 5. Plot of top five optimal ship positions for an eight-cable manipulator, aiming to maximize its workspace.

4. Discussion and conclusions

This study represented a step forward in the application of cable-driven parallel manipulators in subsea operations. It integrates theoretical and practical considerations, focusing on the design and optimization of cable-driven manipulators while emphasizing the necessity of stability for operational safety and precision (Su et al., 2023; Wahba and Honig, 2023). Our research offered valuable workspace analysis, especially pertinent in underwater environments where stability and precision are critical.

The adaptation of the Dykstra algorithm for stabilizing cable tensions in this study introduced an innovative approach in engineering. This adaptation extended its application to underwater robotics, providing a model for addressing complex engineering challenges. Nevertheless, it is important to acknowledge the inherent limitations of the

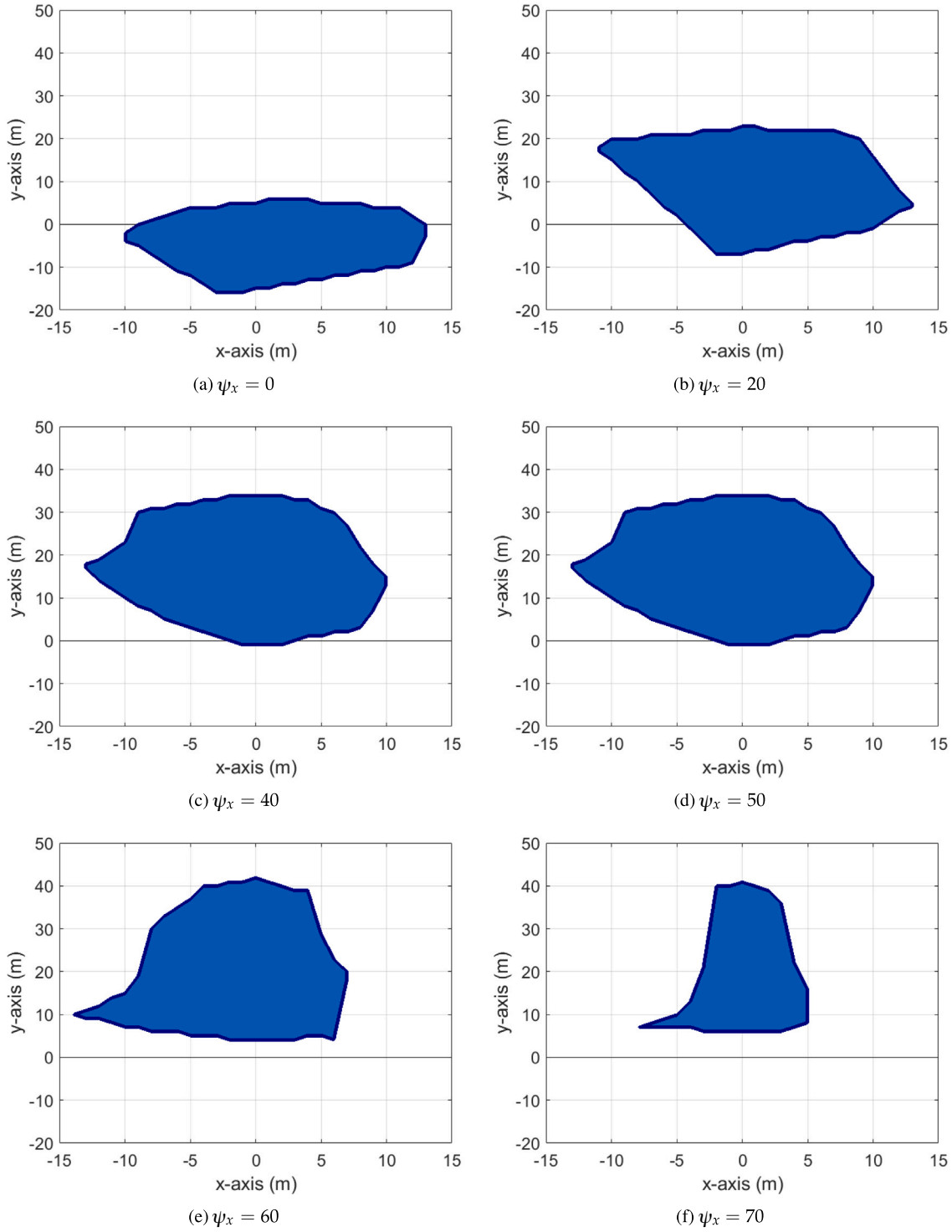

Fig. 6. Manipulator workspace in the x-y plane by variation of the angular orientation ψ_x with $\theta_y = \phi_z = 0$.

Dykstra algorithm. Its iterative nature might necessitate numerous iterations for convergence, particularly in complex scenarios with multiple constraints.

Additionally, the performance of the algorithm is contingent on the selection of initial points and tolerance parameters. While our approach has demonstrated robustness in various scenarios, we acknowledge the potential for further enhancements. Future research will therefore explore alternative or complementary optimization techniques. We aim to undertake comprehensive comparative studies in our subsequent work, evaluating our methodology against other optimization methods and manipulator designs.

This initiative is intended to further validate and refine our approach, enhancing its robustness and broadening its applicability in diverse underwater conditions.

The focus on specific eight- and ten-cable configurations of cable-driven parallel manipulators, though insightful, represents only a subset of potential designs. The reliance on simulation-based findings is a limitation, as real-world complexities might not be fully captured.

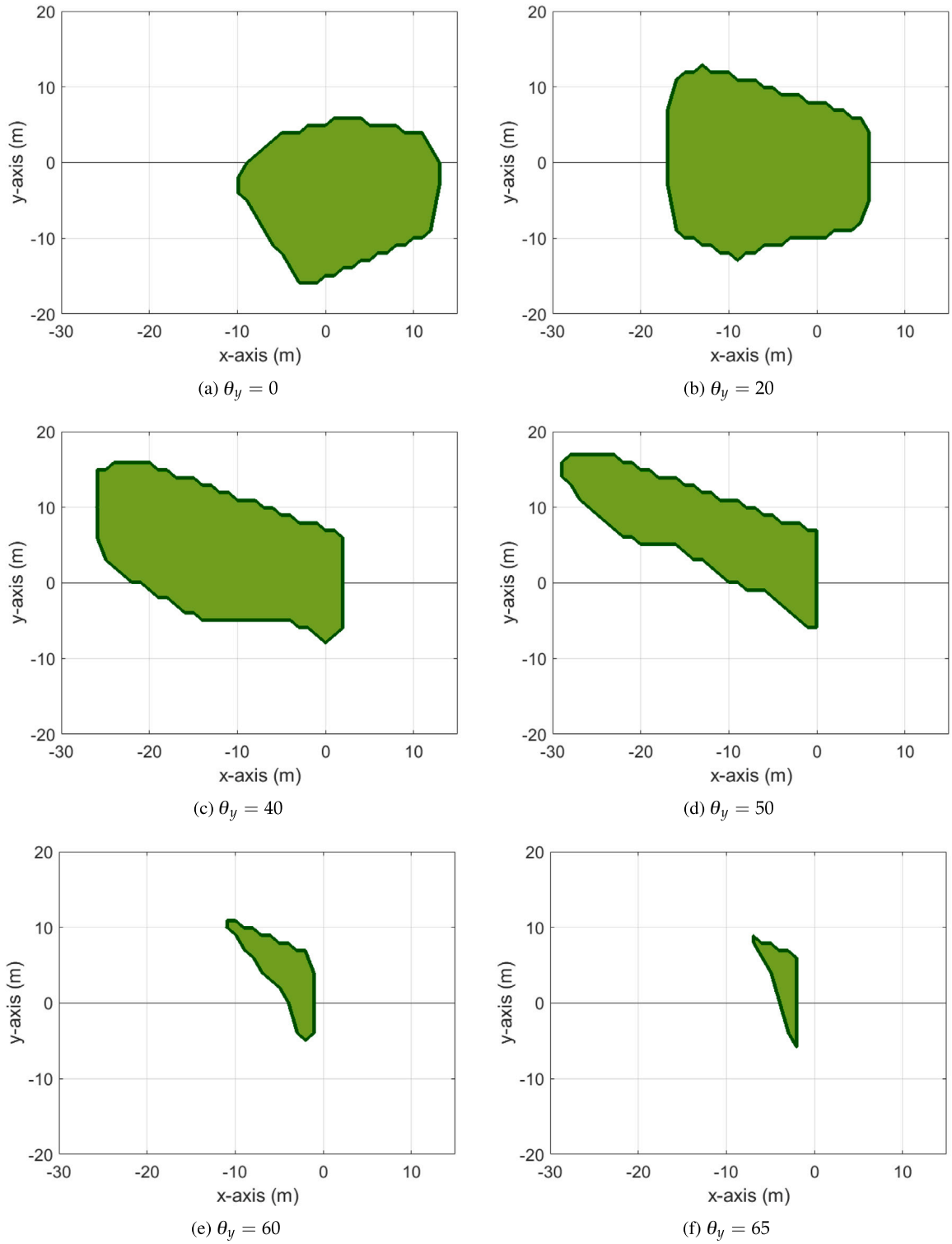

(a) $\theta_y = 0$ (b) $\theta_y = 20$

(c) $\theta_y = 40$ (d) $\theta_y = 50$

(e) $\theta_y = 60$ (f) $\theta_y = 65$

Fig. 7. Manipulator workspace in the x-y plane by variation of the angular orientation θ_y with $\psi_x = \phi_z = 0$.

Experimental validation is therefore needed in future studies to confirm the applicability and scalability of our findings.

Assumptions made in the modeling, such as idealized cable behavior and simplified system dynamics, might impact the real-world applicability of our results. Recognizing this, we emphasize the need for further empirical validation to corroborate the simulation-based outcomes, particularly in real underwater operational conditions.

Future research directions include the application of machine learning, big data, artificial intelligence techniques (Rahman et al., 2023a, 2024; Aykroyd et al., 2019b) to refine optimization algorithms, as well as the use of fuzzy theory and its probabilistic extensions (Rahman et al., 2023a; Kotz et al., 2010) tailoring them to the dynamic and unpredictable nature of underwater environments. Investigating various manipulator configurations and incorporating real-time sensor data could enhance system adaptability and responsiveness to operational conditions. Such advancements could expand the utility and efficacy of cable-driven parallel manipulators across diverse underwater scenarios.

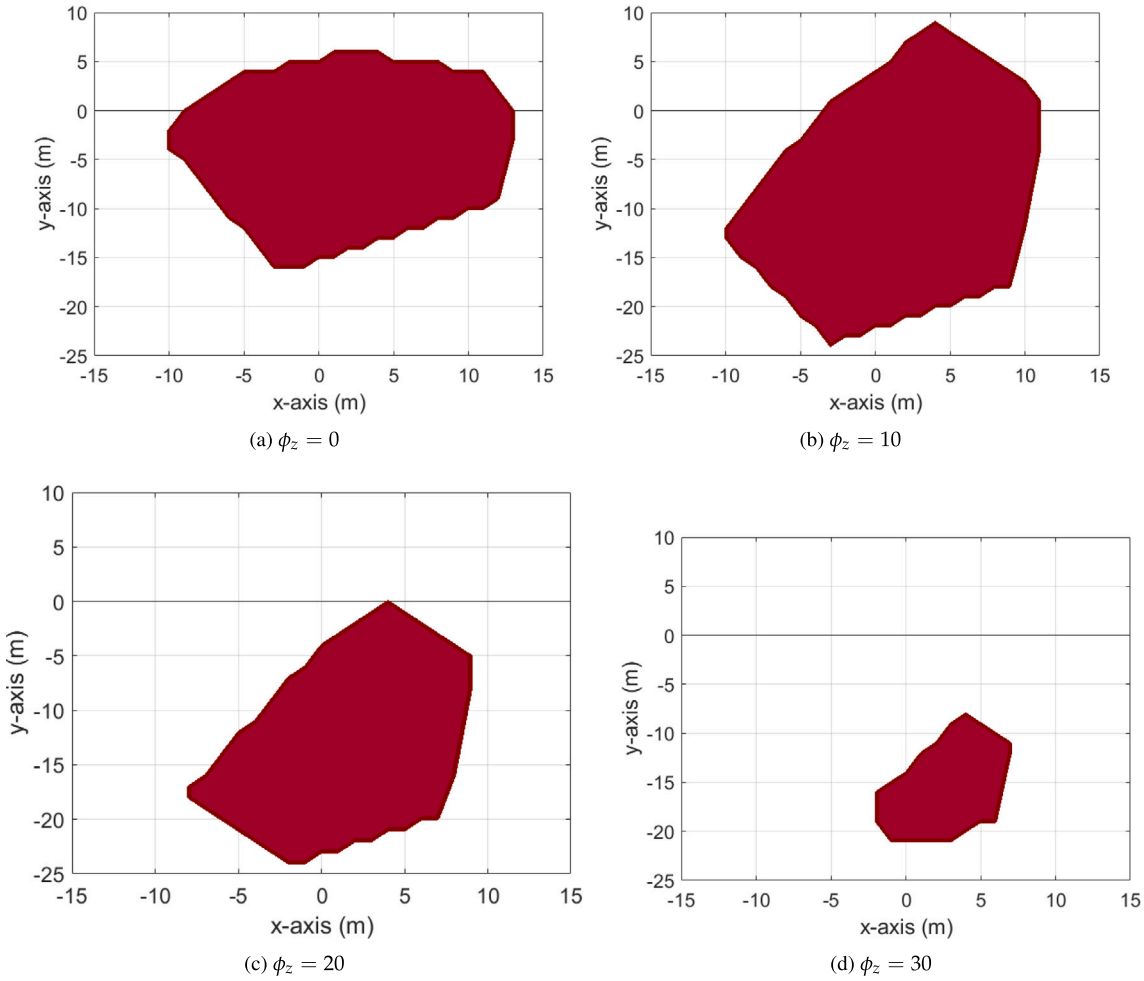

Fig. 8. Manipulator workspace in the x-y plane by variation of the angular orientation ϕ_z with $\psi_x = \theta_y = 0$.

In summary, this study enhances the understanding and application of cable-driven parallel manipulators in marine environments. While acknowledging the theoretical nature of our approach and the need for further empirical validation, particularly in real underwater operational conditions, our research provides a strong foundation for future advancements in this field. Our findings demonstrate the importance of stable cable tensions and effective manipulator design, offering new directions for innovation in underwater robotic systems.

The insights gained from this study are not only applicable to marine applications but also offer new possibilities in the wider field of robotic systems, leading to opportunities for research and practical uses in different areas.

CRediT authorship contribution statement

Asim Ghaffar: Writing – original draft, Validation, Software, Methodology, Investigation, Formal analysis, Data curation, Conceptualization. **Muhammad Zia Ur Rahman:** Writing – original draft, Validation, Software, Methodology, Investigation, Formal analysis, Data curation, Conceptualization. **Víctor Leiva:** Writing – review & editing, Visualization, Validation, Supervision, Methodology, Investigation, Formal analysis, Conceptualization. **Cecilia Castro:** Writing – review & editing, Visualization, Validation, Software, Methodology, Investigation, Formal analysis, Conceptualization.

Declaration of competing interest

The authors declare that they have no known competing financial interests or personal relationships that could have appeared to influence the work reported in the article.

Data availability

Data and codes are available upon request from the authors.

Acknowledgments

The authors would like to thank the editors and reviewers for their constructive comments which led to the improvement of the presentation of the article. Our research was partially funded by FONDECYT, Chile, grant number 1200525,(V. Leiva) from the National Agency for Research and Development (ANID) of the Chilean government under the Ministry of Science, Technology, Knowledge, and Innovation; as well as by Portuguese funds through the CMAT –Research Centre of Mathematics of the University of Minho, Portugal, within projects UIDB/00013/2020 https://doi.org/10.54499/UIDB/00013/2020 and UIDP/00013/2020 https://doi.org/10.54499/UIDP/00013/2020 (C. Castro).

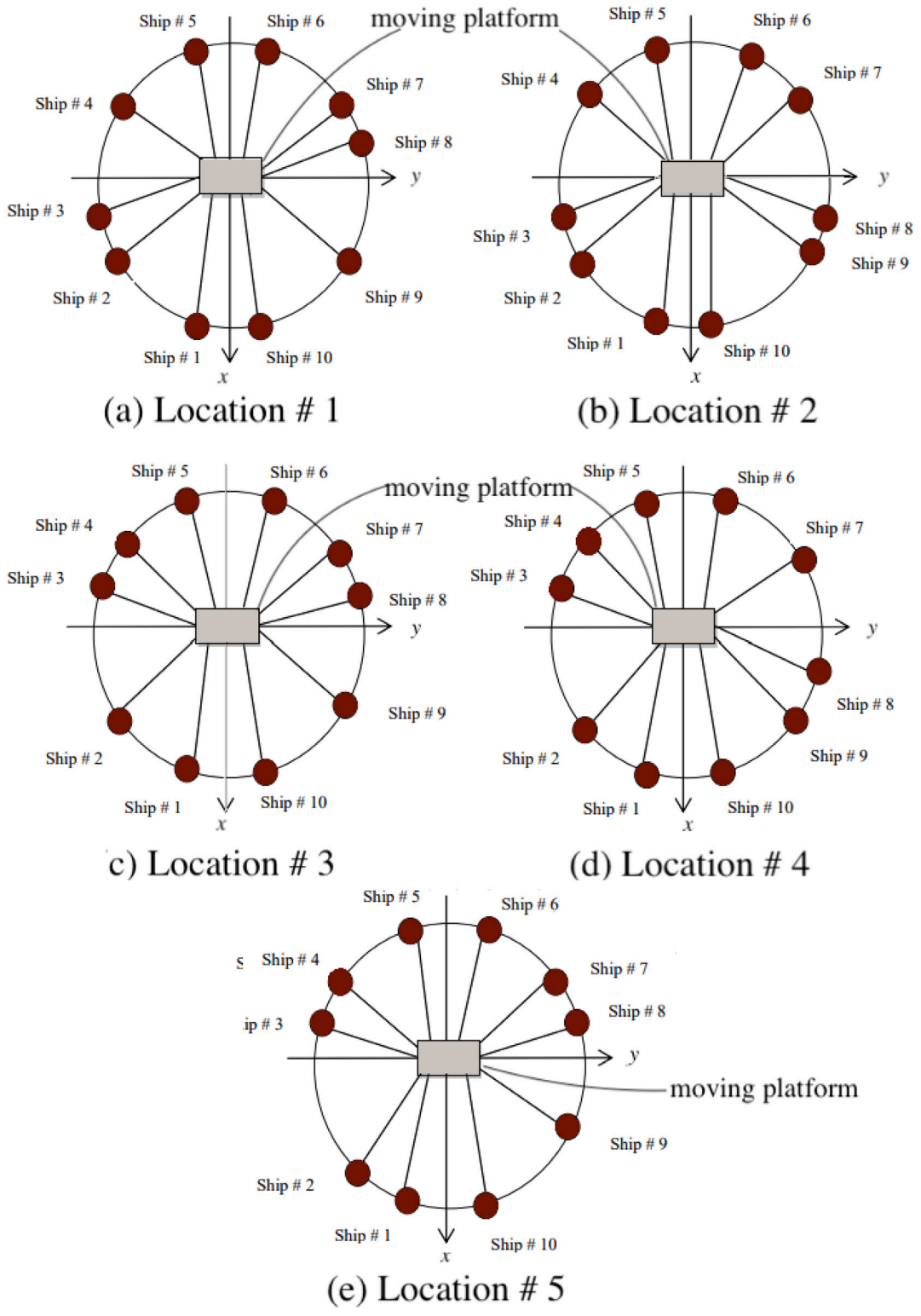

Fig. 9. Plot of top five optimal ship positions for a ten-cable manipulator.

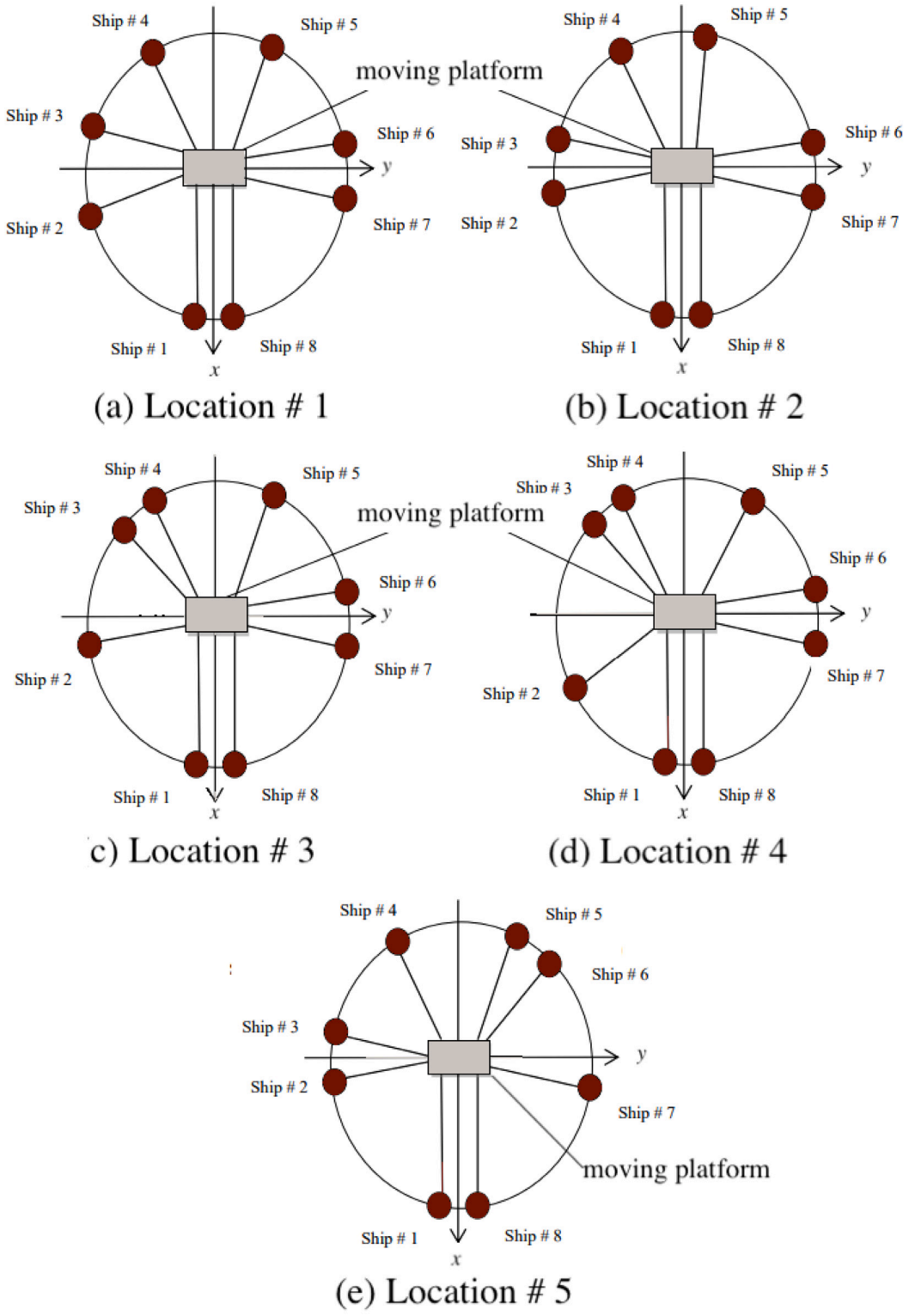

Fig. 10. Plot of top five optimal ship positions for eight-cable manipulator, maximizing stiffness of the system.

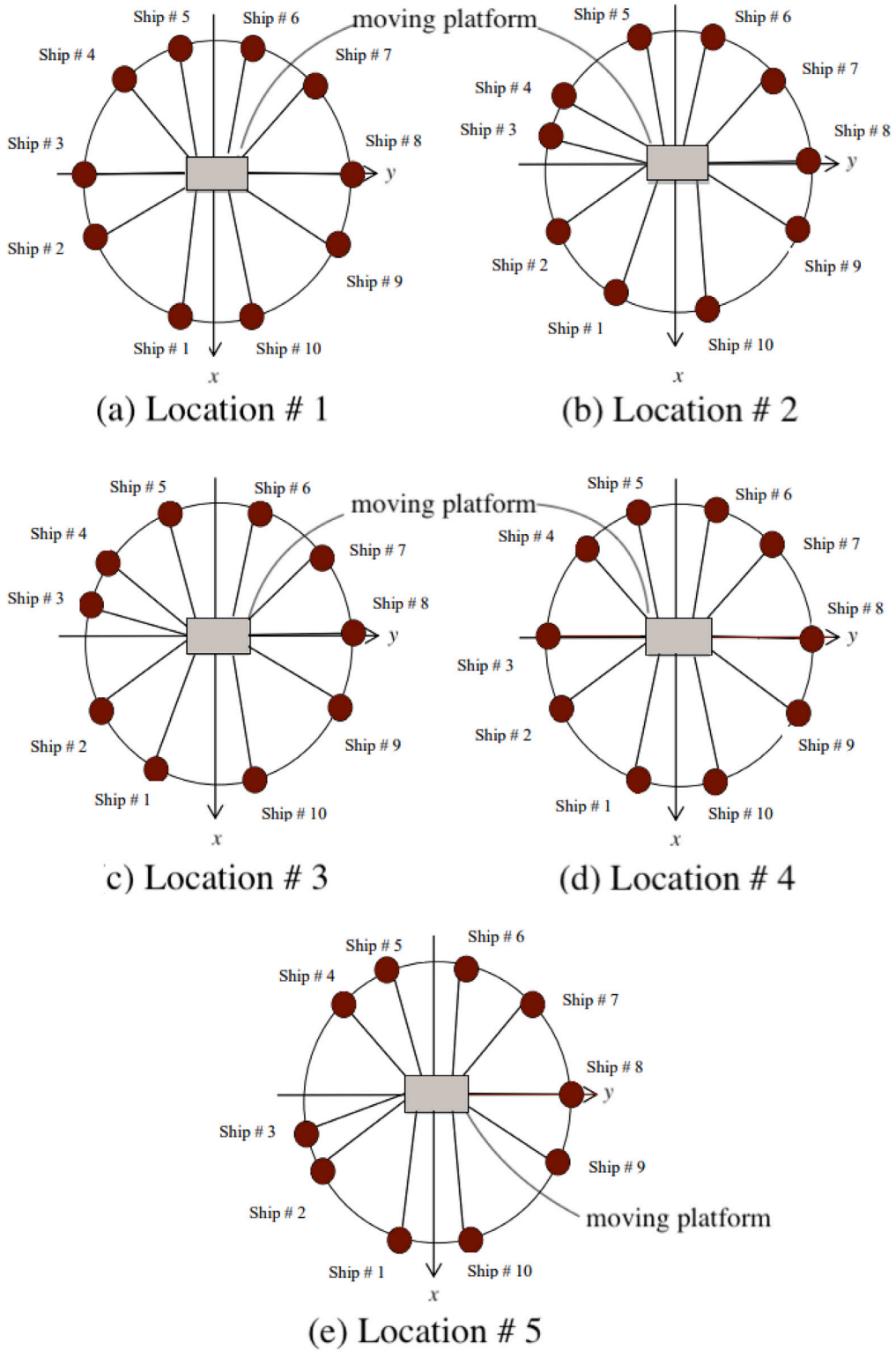

Fig. 11. Plot of top five optimum ship positions for ten-cable manipulator, maximizing stiffness of the system.

References

Ahmad, A., Anderson, K., Sellgren, U., 2011. An approach to stiffness analysis methodology for haptic devices. In: Proceeding of the International Congress on Ultra Modern Telecommunications and Control Systems and Workshops.

Alakhras, A., Sattar, I.H., Alvi, M., Qanbar, M.W., Jaradat, M.A., Alkaddour, M., 2022. The design of a lightweight cable aerial manipulator with a CoG compensation mechanism for construction inspection purposes. Appl. Sci. 12, 1173.

Aykroyd, R.G., Leiva, V., Ruggeri, F., 2019b. Recent developments of control charts, identification of big data sources and future trends of current research. Technol. Forecast. Soc. Change 144, 221–232.

Cui, Z., Tang, X., 2021. Analysis of stiffness controllability of a redundant cable-driven parallel robot based on its configuration. Mechatronics 75, 102519.

Cui, Z., Tang, X., Hou, S., Sun, H., Wang, D., 2019. Optimization design of redundant cable-driven parallel robots based on constant stiffness space. In: Proceedings of the IEEE International Conference on Robotics and Biomimetics. pp. 1041–1046.

Dykstra, R.L., 1983. An algorithm for restricted least squares regression. J. Amer. Statist. Assoc. 78, 837–842.
Ferraresi, C., Paoloni, M., Pastorelli, S., Pescarmona, F., 2004. A new 6-DOF parallel robotic structure actuated by wires: The WiRo-6.3. J. Robot. Syst. 21, 581–595.
Ghaffar, A., Hassan, M., 2014. Study on cable based parallel manipulator systems for subsea applications. In: Proceedings of the Third International Conference on Mechanical Engineering and Mechatronics, vol. 154.
Ghaffar, A., Hassan, M., 2015a. Combined criterion for ship position optimization in cable based parallel manipulators. Appl. Mech. Mater. 736, 211–217.
Ghaffar, A., Hassan, M., 2015b. Failure analysis of cable-based parallel manipulators. Appl. Mech. Mater. 736, 203–210.
Ghaffar, A., Rahman, M.Z.U., Leiva, C., Ali, I., Cabezas, X., Castro, C., 2024. Efficiency, optimality, and selection in a rigid actuation system with matching capabilities for an assistive robotic exoskeleton. Eng. Sci. Technol. Int. J. (in press) available at http://dx.doi.org/10.1016/j.jestch.2023.101613.
Gueners, D., Bouzgarrou, B.C., Chanal, H., 2021. Cable behavior influence on cable-driven parallel robots vibrations: Experimental characterization and simulation. J. Mech. Robot. 13, 041003.
Hamdoun, O., El Bakkali, L., Baghli, F.Z., 2017. Analysis and optimum kinematic design of a parallel robot. Procedia Eng. 181, 214–220.
Hamidi, F., Jerbi, H., Alharbi, H., Leiva, V., Popescu, D., Rajhi, W., 2023. Meta-heuristic solution for stability analysis of nonlinear systems using an intelligent algorithm with potential applications. Fractal Fract. 7, 78.
Hassan, M., Khajepour, A., 2011. Analysis of bounded cable tensions in cable-actuated parallel manipulators. IEEE Trans. Robot. 27, 891–900.
Horoub, M.M., Horoub, A.M., Khan, S., Albalasie, A., Ali, S., Ajamieh, I.A., Alzaydi, A., 2023. Study the effect of changing cables' pattern on the workspace of a six DOF floating parallel marine robot (FPMR). Alex. Eng. J. 64, 847–858.
Jin, X., Ye, W., Li, Q., 2023. New indices for performance evaluation of cable-driven parallel robots: Motion/force transmissibility. Mech. Mach. Theory 188, 105402.
Juárez-Pérez, S., Martín-Parra, A., Arena, A., Ottaviano, E., Gattulli, V., Castillo-García, F.J., 2022. Dynamic control of a novel planar cable-driven parallel robot with a large wrench feasible workspace. Actuators 11, 367.
Kotz, S., Leiva, V., Sanhueza, A., 2010. Two new mixture models related to the inverse Gaussian distribution. Methodol. Comput. Appl. Probab. 12, 199–212.
Maeda, K., Tadokoro, S., Takamori, T., Hiller, M., Verhoeven, R., 1999. On the design of a redundant wire-driven parallel robot WARP manipulator. In: Proceedings 1999 IEEE International Conference on Robotics and Automation (Cat. No. 99CH36288C), vol. 2, pp. 895–900.
Mazzeo, A., Aguzzi, J., Calisti, M., Canese, S., Vecchi, F., Stefanni, S., Controzzi, M., 2022. Marine robotics for deep-sea specimen collection: A systematic review of underwater grippers. Sensors 22, 648.
Muntashir, R., Nurahmi, L., 2022. Reconfiguration of a cable-driven parallel robot based on mobile base position. In: Proceeding of the IEEE International Conference on Mechatronics and Automation.
Nazir, A., Xu, P., Seo, J., 2022. Rock-and-walk manipulation: Object locomotion by passive rolling dynamics and periodic active control. IEEE Trans. Robot. 38, 2354–2369.
Ou, Y., Xu, B., Cai, H., Zhao, J., Fan, J., 2022. An overview of mobile manipulators in nuclear applications. In: Proceeding of the International Conference on Real-time Computing and Robotics. pp. 239–243.
Pierri, F., Nigro, M., Muscio, G., Caccavale, F., 2020. Cooperative manipulation of an unknown object via omnidirectional unmanned aerial vehicles. J. Intell. Robot. Syst. 100, 1635–1649.
Poitrimol, B., Igarashi, H, 2020. Haptic interface for virtual reality based on a hybrid cable-driven parallel robot. In: Proceeding of the IEEE 16th International Workshop, Kristiansand, Norway. pp. 351–356.
Rahman, M.Z.U., Akbar, M.A., Leiva, V., Martin-Barreiro, C., Imran, M., Riaz, M.T., Castro, C., 2024. An IoT-fuzzy intelligent approach for holistic management of COVID-19 patients. Heliyon 10, e22454.
Rahman, M.Z.U., Akbar, M.A., Leiva, V., Tahir, A., Riaz, M.T., Martin-Barreiro, C., 2023a. An intelligent health monitoring and diagnosis system based on the internet of things and fuzzy logic for cardiac arrhythmia COVID-19 patients. Comput. Biol. Med. 154, 106583.
Rahman, M.Z.U., Leiva, V., Ghaffar, A., Martin-Barreiro, C., Waleed, A., Cabezas, X., Castro, C., 2023b. Fractional transformation-based decentralized robust control of a coupled-tank system for industrial applications. Fractal Fract. 7, 590.
Rahman, M.Z.U., Leiva, V., Martin-Barreiro, C., Mahmood, I., Usman, M., Rizwan, M., 2022a. Fractional transformation-based intelligent H-infinity controller of a direct current servo motor. Fractal Fract. 7, 29.
Rahman, M.Z.U., Liaquat, R., Rizwan, M., Martin-Barreiro, C., Leiva, V., 2022b. A robust controller of a reactor electromicrobial system based on a structured fractional transformation for renewable energy. Fractal Fract. 6, 736.
Rahman, M.Z.U., Rizwan, M., Liaquat, R., Leiva, V., Muddasar, M., 2023c. Model-based optimal and robust control of renewable hydrogen gas production in a fed-batch microbial electrolysis cell. Int. J. Hydrogen Energy 48, 30685–30701.
Sawai, K., Aoyama, S., Motoyoshi, T., Oshima, T., Koyanagi, K.I., Masuta, H., Tamamoto, T., 2019. A mobile robot teleoperation system with a wireless communication infrastructure using a leaky coaxial cable based on TCP/IP. Int. J. Adv. Comput. Sci. Appl. 10, 82–89.
Shang, D., Li, X., Yin, M., Zhou, S., 2024. Dynamic modeling and rotation control for flexible single-link underwater manipulator considering flowing water environment based on modified morison equation. Ocean Eng. 291, 116427.
Shen, H., Meng, Q., Li, J., Deng, J., Wu, G., 2021. Kinematic sensitivity, parameter identification, and calibration of a non-fully symmetric parallel delta robot. Mech. Mach. Theory 161, 104311.
Su, Y., Qiu, Y., Liu, P., Tian, J., Wang, Q., Wang, X., 2023. Dynamic modeling, workspace analysis and multi-objective structural optimization of the large-span high-speed cable-driven parallel camera robot. Machines 10, 565.
Tho, T.P., Thinh, N.T., 2022. An overview of cable-driven parallel robots: Workspace, tension distribution, and cable sagging. Math. Probl. Eng. 2022, 2199748.
Wahba, K., Honig, W., 2023. Efficient optimization-based cable force allocation for geometric control of multiple quadrotors transporting a payload. Available at arXiv:2304.02359.
Wang, Z., et al., 2021. Development of a low-inertia 5-DOF hybrid manipulator for moxibustion. In: Proceeding of the 20th International Conference on Advanced Robotics.
Williams, R.L., Graf, E., 2020. Eight-cable robocrane extension for NASA JSC argos. In: Proceedings of the ASME Design Engineering Technical Conference.
Xiong, H., Ma, T., Zhang, L., Diao, X., 2020. Comparison of end-to-end and hybrid deep reinforcement learning strategies for controlling cable-driven parallel robots. Neurocomputing 377, 73–84.
Yue, Y., Li, Y., Zuo, X., 2023. Optimization of subsea production control system layout considering hydraulic fluid pressure loss. Ocean Eng. 288, 116047.
Zarebidoki, M., Dhupia, J.S., Xu, W., 2022. A review of cable-driven parallel robots: Typical configurations, analysis techniques, and control methods. IEEE Robot. Autom. Mag. 29, 89–106.
Zhang, F., Shang, W., Zhang, B., 2020a. Design optimization of redundantly actuated cable-driven parallel robots for an automated warehouse system. IEEE Syst. J. 8, 56867–56879.
Zhang, Z., Shao, Z., Wang, L., 2020b. Optimization and implementation of a high-speed 3-DOFs translational cable-driven parallel robot. Mech. Mach. Theory 145, 103693.